



Universiteit  
Leiden  
The Netherlands

## **T-CYCLE EPR Development at 275 GHz for the study of reaction kinetics & intermediates**

Panarelli, E.G.

### **Citation**

Panarelli, E. G. (2018, December 10). *T-CYCLE EPR Development at 275 GHz for the study of reaction kinetics & intermediates*. *Casimir PhD Series*. Retrieved from <https://hdl.handle.net/1887/68233>

Version: Not Applicable (or Unknown)

License: [Licence agreement concerning inclusion of doctoral thesis in the Institutional Repository of the University of Leiden](#)

Downloaded from: <https://hdl.handle.net/1887/68233>

**Note:** To cite this publication please use the final published version (if applicable).

Cover Page



Universiteit Leiden



The handle <http://hdl.handle.net/1887/68233> holds various files of this Leiden University dissertation.

**Author:** Panarelli, E.G.

**Title:** T-CYCLE EPR Development at 275 GHz for the study of reaction kinetics & intermediates

**Issue Date:** 2018-12-10

**4**

# **Exploring Temperature-Cycle EPR in the sub-second time domain**

### 4.1 Introduction

Being able to investigate chemical kinetics in the sub-second time domain gives access to a great deal of reactions of biological relevance, which occur in a broad range of time domains: from milliseconds to nanoseconds [23], and even down to femtoseconds [76]. Many are the techniques to determine kinetics on the time scale of milliseconds, most notably Rapid Freeze-Quench and flow methods; however, it is the IR-laser-induced temperature-jump techniques that allow – in principle – a considerable downsizing of the accessible time scales in molecular dynamics investigations.

In the previous Chapter, the Temperature-Cycle EPR method was introduced, and demonstrated on a model reaction occurring on a time range of minutes. Bringing about several advantages over other techniques, most importantly the need for one single sample per experiment and therefore the use of a small amount of material, a decisive improvement is needed as far as the time scales within reach are concerned. Since T-Cycle EPR is based on laser-induced T-jumps, in principle the duration of a T-jump can be scaled down by several orders of magnitude as compared to the minute-range obtained in Chapter 3, the main limitation being the heat conductivity of the solutions under study.

The present Chapter is devoted to the application of T-Cycle EPR on a model reaction that takes place over several hundreds of milliseconds, using a similar setup as described in the previous Chapter. A new hand-mixing method is described to easily and efficiently mix the reagents without them reacting. Furthermore, quantitative kinetics can be obtained provided an analysis of the sample's temperature profile during the laser pulse is performed, which also yields the effective reaction time per T-jump, and the dependence of the rate constant on temperature.

### 4.2 Experimental

#### 4.2.1 Materials and setup

Oxygen-free mixtures of TEMPOL (4-hydroxy-TEMPO, Sigma-Aldrich, cat. n. 176141) and sodium dithionite ( $\text{Na}_2\text{S}_2\text{O}_4$ , sodium hydrosulphite 85%, Sigma-Aldrich, cat. n. 15,795-3) used for the T-Cycle experiments in this Chapter were prepared from batch solutions at concentrations of 2 and 100 mM, respectively, in a mixture of phosphate buffer and glycerol 1:1 in volume. In view of the high reactivity of sodium dithionite with oxygen [77], both the TEMPOL and buffer batch solutions, together with the sodium dithionite powder prior to dissolution, were bubbled with argon for at least one hour while kept in air-tight vials sealed with rubber septa caps, to

#### 4. EXPLORING TEMPERATURE-CYCLE EPR IN THE SUB-SECOND TIME DOMAIN

---

ensure a complete removal of oxygen. In order to transfer the buffer:glycerol solution into the vial containing the sodium dithionite powder, and to transfer the de-oxygenated solutions to the beaker for the mixing (see Subsection 4.2.3), a Hamilton air-tight syringe was employed.

The phosphate buffer solution had a concentration of 120 mM and a pH of 7.0, and was prepared from stock solutions of sodium phosphate monobasic (G-Biosciences, cat. n. RC-098) and sodium phosphate dibasic (Sigma-Aldrich, cat. n. S5136-1KG) dissolved in Milli-Q water; glycerol was purchased from Sigma-Aldrich (puriss., cat. n. 15523-1L-R).

Resulting concentrations of TEMPOL and sodium dithionite of 1 and 50 mM respectively were then obtained upon hand mixing with the special technique explained in Subsection 4.2.3.

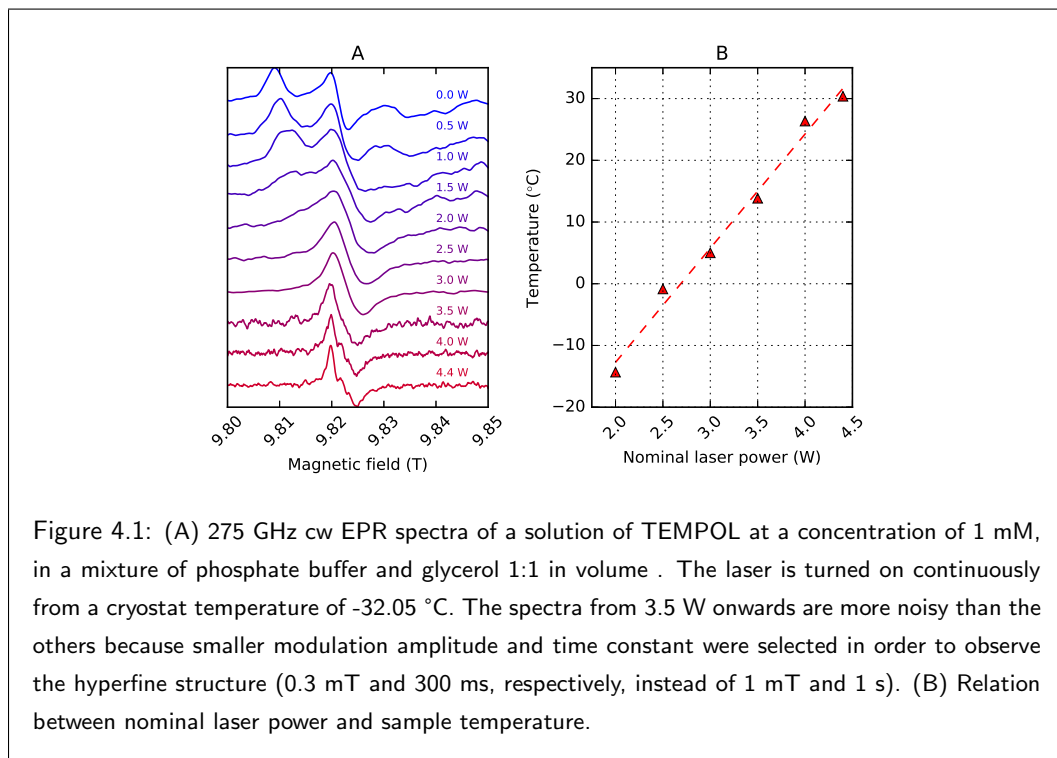
MnCl<sub>2</sub> at a concentration of 10 μM was added to both solutions prior to mixing, to be used as an internal standard. Details on the practice of using Mn<sup>2+</sup> as a standard are provided in Chapter 3.

The samples are introduced in the single-mode cavity of a pre-cooled home-built probe head in a similar way as described in Chapter 2 of this thesis. Like described in Chapter 3, the probe head is then inserted in the He-flow cryostat of a home-built 275 GHz EPR spectrometer at a measurement temperature of 243 K.

The T-Cycle setup is essentially the same one as described in Chapter 3, except for a few modifications, such as the multi-mode optical fiber (Thorlabs, model n. FG200LCC, 0.22 NA, core size 200 μm, HPSMA connector to the laser) and the 4.4-W diode laser (SemiNex Corp., model n. 15P-110, serial n. 7559). With this setup, the behavior of a solution of TEMPOL in a mixture of buffer and glycerol is reported in Figure 4.1 A as a function of nominal laser power, in the range between 0.5 and 4.4 W. By employing the relation between spectral "partial linewidth" and temperature illustrated in the Appendix to Chapter 3, it is possible to link the nominal laser power to the temperature reached by the sample, as shown in Figure 4.1 B (here, this is possible in the range between 2.0 and 4.4 W). With this arrangement, the maximum T-jump obtained is ~ 60 °C at 4.4 W nominal laser power from a starting temperature of ~ -30 °C, in contrast with a maximum T-jump of ~ 120 °C at 3.5 W reported for the setup of Chapter 3.

Laser-induced T-jumps were applied with pulses of the length of either 50 or 100 ms. The pulse duration was controlled by an electronic clock that triggered the current fed to the diode laser. Since the rise and fall time of the laser-induced T-jump on the sample are long as compared to the duration of the pulses applied here, which therefore do not allow the system to reach a steady state, an analysis of the temperature profile of the sample during the T-jump is required in order to determine quantitative kinetics (see Subsection 4.3.2).

#### 4. EXPLORING TEMPERATURE-CYCLE EPR IN THE SUB-SECOND TIME DOMAIN



The time profiles shown in Subsection 4.3.2 were obtained with an oscilloscope (LeCroy WaveSurfer 424), by measuring the 275 GHz EPR intensity of a solution of TEMPOL at the fixed magnetic field of 9.8197 T as a function of time, while applying laser pulses of a length of either 100 or 500 ms with a repetition time of 3 s. The oscilloscope window was set to 50 mV/div and 100 ms/div, and the signal was averaged 1600 times, because of the high noise level caused by the spectrometer's time constant of 3 ms used to record the time profiles. The TEMPOL solution was kept in the spectrometer's cryostat at a temperature of 243 K, at a concentration of 3 mM, in a mixture of glycerol and phosphate buffer (120 mM, pH 7.0), 1:1 in volume. The EPR parameters are the same as reported in Table 4.1; however, when recording a spectrum with the laser on, a smaller modulation amplitude and time constant were used, of 0.3 mT and 0.3 s, respectively.

The simulations shown in Section 4.4 were made with the COMSOL Multiphysics software (v. 5.3 a), performing a time-dependent study of the sample's temperature (0 to 1500 ms, with steps of 10 ms) with the package for heat transfer in fluids. To model the experimental conditions, a simplified geometry made up of an ensemble of five cylinders was created (see Figure 4.10).

Further details on their sizes and explanations on their meaning in the model are provided in Subsection 4.4.1. As far as the meshing is concerned, since the interesting temperature variations to simulate were those of the sample, the size of the meshing patterns were set differently for the sample cylinder ("Extremely Fine" mesh) as compared to the other cylinders ("Fine" mesh for the quartz cylinder, "Coarse" or "Normal" mesh for the helium cylinders inside the quartz, and "Extremely Coarse" mesh for the bigger helium cylinder). In all cases, the meshes were automatically generated with the program's "physics-controlled" algorithm. The physical properties as a function of temperature needed to perform the simulations (i.e., heat capacity at constant pressure, density, thermal conductivity, and dynamic viscosity) were taken automatically from the COMSOL Multiphysics library for quartz and helium; the properties of the mixture of water and glycerol 1:1 in volume had to be specified manually and were obtained from [74].

### 4.2.2 The TEMPOL-dithionite reaction

The reduction of TEMPOL by sodium dithionite is a well-established reaction employed in millisecond-scale kinetic EPR studies [78] [79] [66]. With a much higher concentration of sodium dithionite ( $[S_2O_4^{2-}]$ ) over TEMPOL ( $[TL]$ ), the reaction exhibits a pseudo-first-order behavior, as expressed in Equation 4.1 (after [66]):

$$\frac{d[TL]}{dt} = k' \cdot [TL] \quad (4.1)$$

$$k' = k \cdot [S_2O_4^{2-}] \quad (4.2)$$

with  $k'$  being the apparent rate constant. Sodium dithionite is known to undergo a dissociation equilibrium that produces the sulfonyl radical anion,  $SO_2^{\bullet-}$ , which gives a sharp EPR signal at  $g = 2.0057$  [79]. Since the EPR signal of  $SO_2^{\bullet-}$  overlaps with the  $g_y$ -component of the spectrum of TEMPOL around 9.82 T, the  $g_x$ -component around 9.81 T was chosen instead to follow the reaction.

### 4.2.3 Sub-zero mixing

Since the reduction of TEMPOL by dithionite unfolds within milliseconds, simple hand mixing of the two components at room temperature is not possible. A convenient feature of mixtures of pure water and glycerol is their low freezing point, which makes them highly viscous fluids at temperatures well below 0 °C [74]. Based on such property, for the experiments described in this Chapter a mixing method was devised, henceforth referred to as "sub-zero mixing", that

#### 4. EXPLORING TEMPERATURE-CYCLE EPR IN THE SUB-SECOND TIME DOMAIN

allows an effective and simple hand mixing of the solutions of TEMPOL and sodium dithionite at a temperature of roughly  $-50\text{ }^{\circ}\text{C}$ , i.e., well below the temperature at which the mixture starts to react.

A 5-mL Pyrex beaker is kept inclined at about  $45^{\circ}$  and immersed in liquid nitrogen. A volume of  $150\text{ }\mu\text{L}$  of one reagent is transferred into the inclined side of the beaker, as shown in Figure 4.2 A. Upon freezing of the solution, the beaker is inclined on the other side (while still being kept in liquid nitrogen), and a volume of  $150\text{ }\mu\text{L}$  of the other reagent is transferred into that side, where it freezes. Care is taken to avoid the two solutions to ever be in physical contact, as shown in Figure 4.2 B. The beaker is then transferred in a setup very similar to that described in Chapter 2, namely a polystyrene box partly filled with liquid nitrogen, having a metal plate in it, secured on top of an octagonal polystyrene box. On the metal plate stands a 3.5-cm-high metal slab, on top of which is placed the 5-mL beaker containing the separated frozen solutions. By optimizing the level of liquid nitrogen in the polystyrene box (with a filling level of about 2 cm), and the flow of cold gaseous nitrogen blowing on the liquid nitrogen (which keeps the temperature immediately above the metal plate at about  $-50\text{ }^{\circ}\text{C}$ ), the metal slab stabilizes at a temperature of about  $-60\text{ }^{\circ}\text{C}$ , and the frozen solutions in the beaker warm up from liquid-nitrogen temperature to about  $-50\text{ }^{\circ}\text{C}$ . At this temperature, the solutions have a toothpaste-like texture, and can easily be mixed with a pre-cooled spatula. The reagents are thus efficiently mixed at a temperature where no reaction occurs (Figure 4.2 C).

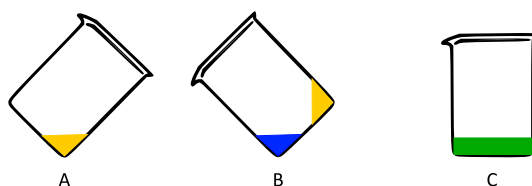


Figure 4.2: Scheme of steps for the sub-zero mixing. One reagent solution (depicted in yellow) is dropped on one side of the inclined beaker, where it freezes being at liquid nitrogen temperature (A). The other reagent solution (depicted in blue) is then dropped on the other side of the inclined beaker, and let to freeze (B). The beaker is finally placed on a metal slab, where it reaches a temperature of  $-50\text{ }^{\circ}\text{C}$ , and it is possible to mix the two solutions (C).

Quartz capillaries connected to a syringe, prepared and handled in a similar way as described in Chapter 2 of this thesis, are then used to suck the cold mixture of reagents up to the silica-gel

filter in the capillary. Once filled, the capillary is transferred in a metal block (described in Chapter 2), and is then stored in dry ice for later measurements. The capillary is finally loaded in the pre-cooled spectrometer probe head following the procedure described in Chapter 2.

## 4.3 Results

This Section reports the 275 GHz cw EPR spectra obtained from applying the Temperature-Cycle method on a mixture of TEMPOL and sodium dithionite (experimental parameters are provided in Table 4.1), and the resulting subsecond-range decay. Similarly to Chapter 3, the spectral peak around 9.81 T was monitored, and the function  $Y(t)$  was calculated versus time through normalization with the  $Mn^{2+}$  signal around 9.8408 T. See Chapter 3 also for the interpretation of the 275 GHz EPR spectra of TEMPOL. Whenever shown, error bars are calculated from the standard error on the four scans that are averaged. The standard error is calculated as follows:

$$e_n = \sqrt{\frac{1}{M_n} \sum_{m=1}^{M_n} (Y_{n,m} - \langle Y_n \rangle)^2} \quad (4.3)$$

where  $Y_{n,m}$  is the value of  $Y$  for the  $m$ -th scan of the  $n$ -th point in time,  $\langle Y_n \rangle$  is the averaged value of  $Y$  of the  $n$ -th point in time, and  $M_n$  is the total number of scans of the  $n$ -th point. Expressing the errors in this way represents the EPR intensity variation from scan to scan, which – except for a few points – outweighs the noise level.

Field range (T)	# of points	Mod. freq. (kHz)	Mod. ampl. (mT)	Time const. (s)	Conversion time (s)	Microwave power ( $\mu$ W)	T (K)
9.8 ÷ 9.855	1100	1.253	1.0	1	0.125	1.74	243

Table 4.1: Experimental parameters of the cw spectra at 275 GHz. *Mod. freq.* and *Mod. ampl.* are the field modulation frequency and amplitude, respectively.

### 4.3.1 Temperature-Cycle EPR on a sub-second time scale

In the experiment described here, Temperature-Cycle EPR is applied on a mixture of TEMPOL and sodium dithionite, prepared with the "sub-zero mixing" described in the previous Section. The sub-zero mixing ensures that the two reagents have not reacted during the mixing prior to exposure to the laser-induced T-jumps, so that the reaction is effectively observed from  $t = 0$ . Furthermore, the mixture is kept at a cryostat temperature of  $-30$  °C, which prevents the reaction

## 4. EXPLORING TEMPERATURE-CYCLE EPR IN THE SUB-SECOND TIME DOMAIN

---

to occur. A sequence of T-jumps, obtained by turning the laser on for a duration of either 50 or 100 ms at a nominal power of 4.4 W, is then applied on the mixture, and the reduction of TEMPOL by dithionite can be followed by measuring the 275 GHz EPR spectral intensity of the sample after each laser pulse.

The result is a decay of the 275 GHz EPR intensity of TEMPOL as a function of the laser time. As shown in Figure 4.3 A, a progressive decrease of the intensity of the TEMPOL spectrum is observed (red to fuchsia spectra), until no signal is detected anymore except for the lines from  $\text{Mn}^{2+}$ , thus showing that a spectral decay can be obtained when applying T-Cycle EPR with laser pulses of a duration well below the second. By plotting the  $Y(t)$  function, calculated from the  $g_x$  spectral component of TEMPOL, an intensity decay can be observed on the laser-time axis up to 1850 ms, as shown in Figure 4.3 B. The five points after the first one in the decay of Figure 4.3 B correspond to laser pulses of a duration of 50 ms, while the later ones correspond to laser pulses of a duration of 100 ms.

Since the rise time of a T-jump lasts at least 300 ms (as described in Chapter 3), the system in the present experiment does not reach an equilibrium temperature during the time the laser is turned on. In order to determine the time that the sample effectively spends above a temperature where it starts to react, an analysis of the temperature profile of the sample during the application of a laser pulse is required.

### 4.3.2 Quantitative analysis of the sub-second kinetics

In Chapter 3 of this thesis, it was described how, upon turning the laser on for a relatively long time, it takes the sample at least 300 ms to reach an equilibrium temperature. In the experiments described in the present Chapter, however, the laser is turned on for a considerably shorter time (50 or 100 ms). The sample therefore does not have the time to reach an equilibrium temperature while the laser is on. This poses a twofold difficulty; firstly, on the actual time the sample spends at the reaction temperature, and secondly, on the definition of the reaction temperature itself, given that no steady state is ever reached during the T-jump. Hereinafter is the description of a method to determine the effective time that the sample spends at a temperature where the reaction occurs, upon application of a laser pulse of the duration of 100 ms. This method allows to calculate the reaction rate's dependence on temperature, and provides a way to estimate the reaction's activation energy. The idea at the basis of the method is that of assigning the EPR intensity variations of TEMPOL as a function of temperature (determined by recording a cw spectrum at different cryostat temperatures), to the intensity variations as a function of time (recorded with an oscilloscope), obtained by applying laser pulses of 100 ms on the sample. As

#### 4. EXPLORING TEMPERATURE-CYCLE EPR IN THE SUB-SECOND TIME DOMAIN

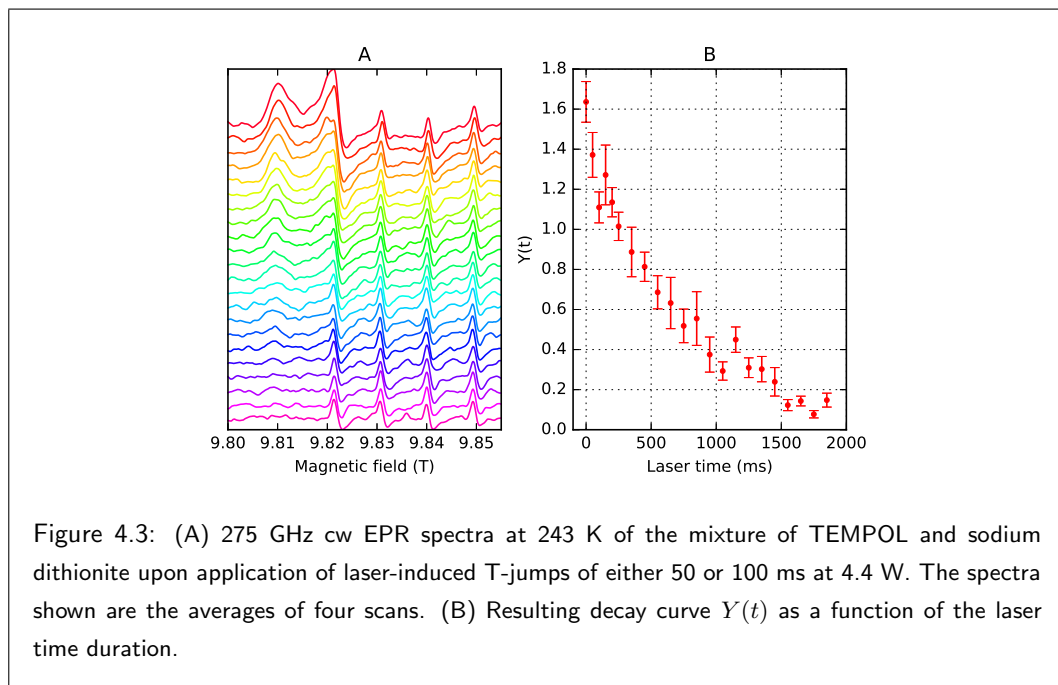


Figure 4.3: (A) 275 GHz cw EPR spectra at 243 K of the mixture of TEMPOL and sodium dithionite upon application of laser-induced T-jumps of either 50 or 100 ms at 4.4 W. The spectra shown are the averages of four scans. (B) Resulting decay curve  $Y(t)$  as a function of the laser time duration.

a result, by taking into account the fact that the temperature of the sample changes during the application of the laser pulse (since an equilibrium temperature is not reached), the rate constant as a function of temperature can be modeled quantitatively, and the reaction's activation energy can be estimated. Furthermore, it is possible to determine the time that the sample effectively spends at a temperature at which the reaction takes place (which is shorter than the nominal 100 ms of the laser pulse application).

The 275 GHz EPR spectral changes of a solution of TEMPOL (in the absence of sodium dithionite) as a function of temperature are shown in Figure 4.4 A, where spectra are obtained at several cryostat temperatures in the range between  $\sim -33$  and  $+28$  °C. Details about the causes of such behavior are provided in the Appendix to Chapter 3. By sitting on a fixed magnetic field, it is possible to plot the spectral intensity at that field as a function of temperature; this is shown for four different values of magnetic field in Figure 4.4 B. It can be appreciated how the EPR intensity at the field of 9.8197 T (blue triangles) is particularly sensitive to temperature variations in the range between  $\sim -20$  and  $+30$  °C, as compared to the curves at other fields. This specific field value was thus chosen to characterize the temperature profile associated to the 100 ms laser pulse.

#### 4. EXPLORING TEMPERATURE-CYCLE EPR IN THE SUB-SECOND TIME DOMAIN

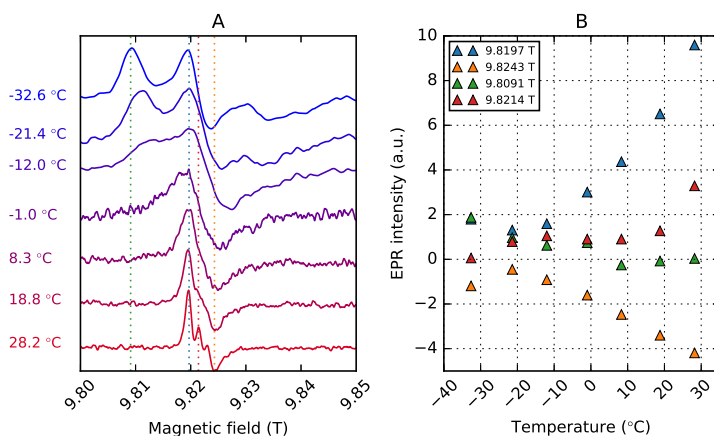


Figure 4.4: (A) 275 GHz spectra as a function of the cryostat temperature of a 1-mM solution of TEMPOL in a mixture of glycerol and phosphate buffer (120 mM, pH 7.0), 1:1 in volume. The colored dotted lines show the magnetic field values at which the spectral intensities are taken and plotted as a function of temperature, in (B). Notice that in (A) each spectrum is normalized within the range 0 to 1, while the intensities in (B) are from the actual experimental spectral intensities.

With an oscilloscope, the 275 GHz EPR intensity variation of a solution of TEMPOL at the fixed magnetic field of 9.8197 T was measured while applying 100 ms long laser pulses at a nominal power of 4.4 W. Figure 4.5 A shows the raw time profile (profile on top), the baseline time profile recorded at a magnetic field of 9.8 T (i.e., without an EPR signal, profile in the middle), and the difference of the two (profile at the bottom). The baseline correction is essential to obtain a time profile without the disturbance effects induced by the laser pulse on the spectrometer's cavity, which last even longer than the duration of the pulse itself. By comparing the corrected time profile of Figure 4.5 A (bottom) and the curve at 9.8197 T of Figure 4.4 B (blue triangles), a consistent trend can be appreciated; furthermore, it can be visualized that with a laser pulse of the duration of 100 ms the sample does not reach an equilibrium temperature, because the laser is switched off before an intensity plateau is attained.

In order to associate the EPR intensity variations at 9.8197 T from Figure 4.4 B (blue triangles) to the time profile of Figure 4.5 A (bottom), a comparison is made between the latter and a time profile with a longer laser pulse, which enables the sample to reach an equilibrium temperature. The green profile of Figure 4.5 B, obtained by applying laser pulses of 500 ms at the same nominal power of 4.4 W, shows that the sample reaches an equilibrium temperature

#### 4. EXPLORING TEMPERATURE-CYCLE EPR IN THE SUB-SECOND TIME DOMAIN

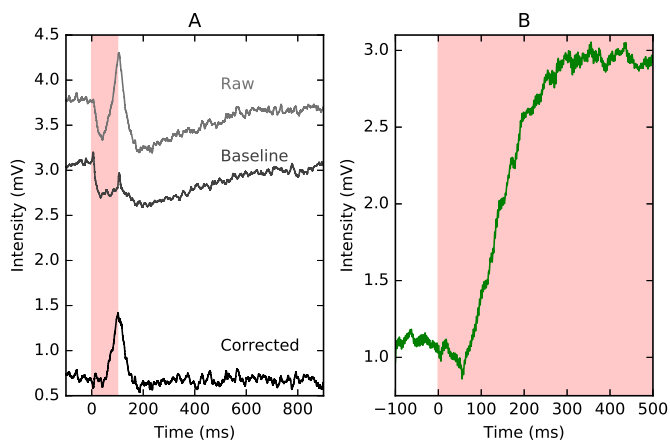


Figure 4.5: Time profiles of the 275 GHz EPR spectral intensity at the magnetic field of 9.8197 T of a 3-mM solution of TEMPOL in a mixture of glycerol and phosphate buffer (120 mM, pH 7.0), 1:1 in volume. (A) Upon application of 100 ms long laser pulses at a nominal power of 4.4 W. The raw time profile (light gray) is corrected by the baseline time profile (dark gray) recorded at the magnetic field of 9.8 T. (B) Upon application of 500 ms long laser pulses, at the same power. This time profile was corrected by the baseline time profile from (A).

after about 300 ms from the beginning of the laser pulse. The baseline profile corresponding to the green profile was not measured, so that the laser's disturbance effects on the cavity are partly visible at the beginning of the profile; however, the profile's baseline level was shifted by the baseline of the profile at 100 ms from Figure 4.5 A.

The equilibrium temperature corresponding to the intensity plateau of the 500 ms profile is straightforwardly obtained by measuring the cw EPR spectrum of the sample with the laser continuously on, which yields the spectrum A of Figure 4.6. The good match with the spectrum at +28.2 °C from the temperature calibration of Figure 4.4, reported as spectrum B in Figure 4.6, confirms the equilibrium temperature of the 500 ms pulse to be around +30 °C. Figure 4.6 also compares spectrum C, corresponding to the baseline of the time profiles of Figure 4.5 (recorded at -32.0 °C with the laser off) with the spectrum at -32.6 °C from the temperature calibration, here presented as spectrum D. Once again, the good match confirms the starting temperature of the profile of Figure 4.5 to be around -30 °C.

The baseline level of the profile of Figure 4.5 A (bottom) therefore corresponds to the intensity of the point at -32.6 °C of Figure 4.4 B (blue triangles); the value of this initial intensity is assigned

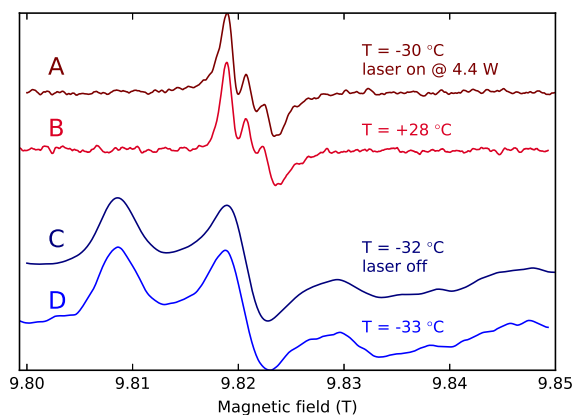
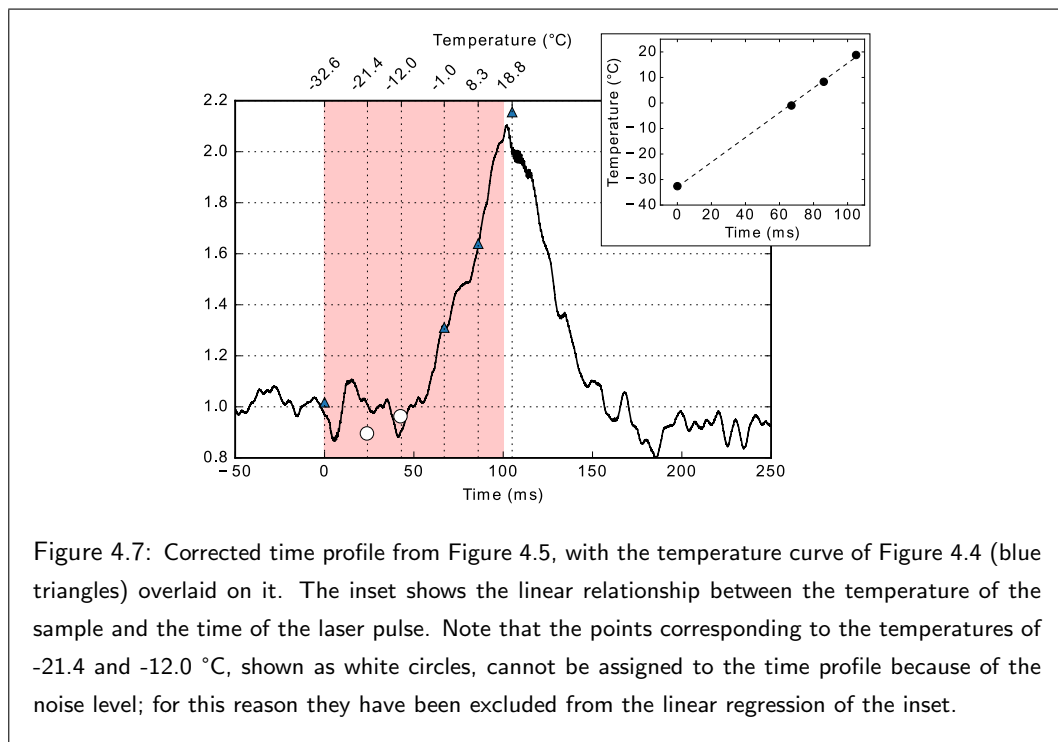


Figure 4.6: Comparison of 275 GHz spectra of TEMPOL in solution with a mixture of glycerol and phosphate buffer (120 mM, pH 7.0), 1:1 in volume. (A) and (C) correspond to the experiment shown in Figure 4.5, recorded, respectively, at a temperature of  $-30.2\text{ }^{\circ}\text{C}$  with the laser continuously on at a nominal power of 4.4 W, and of  $-32.0\text{ }^{\circ}\text{C}$  with the laser off. (B) and (D) correspond, respectively, to the first (at  $-32.6\text{ }^{\circ}\text{C}$ ) and the last (at  $+28.2\text{ }^{\circ}\text{C}$ ) spectrum of the temperature calibration of Figure 4.4.

to 1 mV in the scale of Figure 4.5. Moreover, the plateau of the green profile of Figure 4.5 B corresponds to the intensity of the point at  $+28.25\text{ }^{\circ}\text{C}$  of Figure 4.4 B (blue triangles), i.e., to a value of about 3 mV in the scale of Figure 4.5. In this way, the curve at 9.8197 T of Figure 4.4 (blue triangles) can be overlaid on the profile of Figure 4.5 A, and the temperature variations can then be associated to the time scale, as shown in Figure 4.7. Although the points at  $-21.4$  and  $-12.0\text{ }^{\circ}\text{C}$  (depicted as white circles) can only be tentatively associated to the time profile because of the noise level, the points from  $-1.0$  to  $+18.8$  are matching well the intensity change of the time profile within the laser pulse, and are linearly related to the initial point at  $-32.6\text{ }^{\circ}\text{C}$ . The inset of Figure 4.7 shows the linear behavior of these temperatures as a function of the time of the laser pulse.

In order to understand how long a time interval the sample spends at temperatures at which the reaction actually takes place within the time scale of milliseconds, a slower decay of the reduction of TEMPOL by dithionite is considered. Although the experimental conditions employed to obtain this decay are the same as described in this Chapter, the T-Cycle setup was different, namely different models of the optical fiber, diode laser, and fiber connector were used

#### 4. EXPLORING TEMPERATURE-CYCLE EPR IN THE SUB-SECOND TIME DOMAIN



as compared to those reported here.

Figure 4.8 A reports such decay, showing a complete depletion of the TEMPOL signal within 40 s, upon application of laser pulses of the duration of 5 s (20 s for the last point) at a nominal power of 2.0 W. Since the laser pulses are much longer than the rise time, at each point the sample does reach a steady temperature which is also the reaction temperature, determined to be  $\sim 8$  °C by comparing the spectrum of a solution of identical composition (but without sodium dithionite) with the laser continuously on (a in Figure 4.8 B), with the spectrum at 8.3 °C from the temperature calibration of Figure 4.4, here shown as spectrum b. Figure 4.8 B also compares the spectrum of the sample at the starting temperature of  $-30$  °C (spectrum c) with the one at the same temperature from the temperature calibration (spectrum d), showing a good match and thus confirming the starting temperature. From the fit of the decay of Figure 4.8 A, a rate  $k(8^\circ\text{C}) = 2.0 \pm 0.2 \text{ M}^{-1} \text{ s}^{-1}$  is calculated.

The time interval that the sample spends at a temperature greater than or equal to 8 °C appears to be about 40 ms from Figure 4.7. With the aforesaid rate at 8 °C of  $2.0 \text{ M}^{-1} \text{ s}^{-1}$ , the intensity change of the TEMPOL signal is less than 1% within the time window of 40 ms.

#### 4. EXPLORING TEMPERATURE-CYCLE EPR IN THE SUB-SECOND TIME DOMAIN

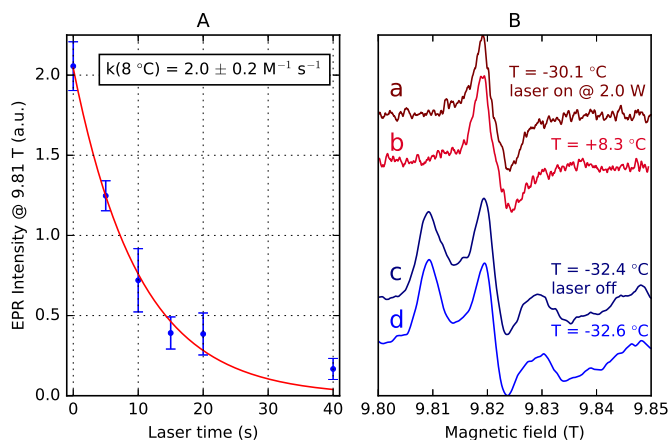
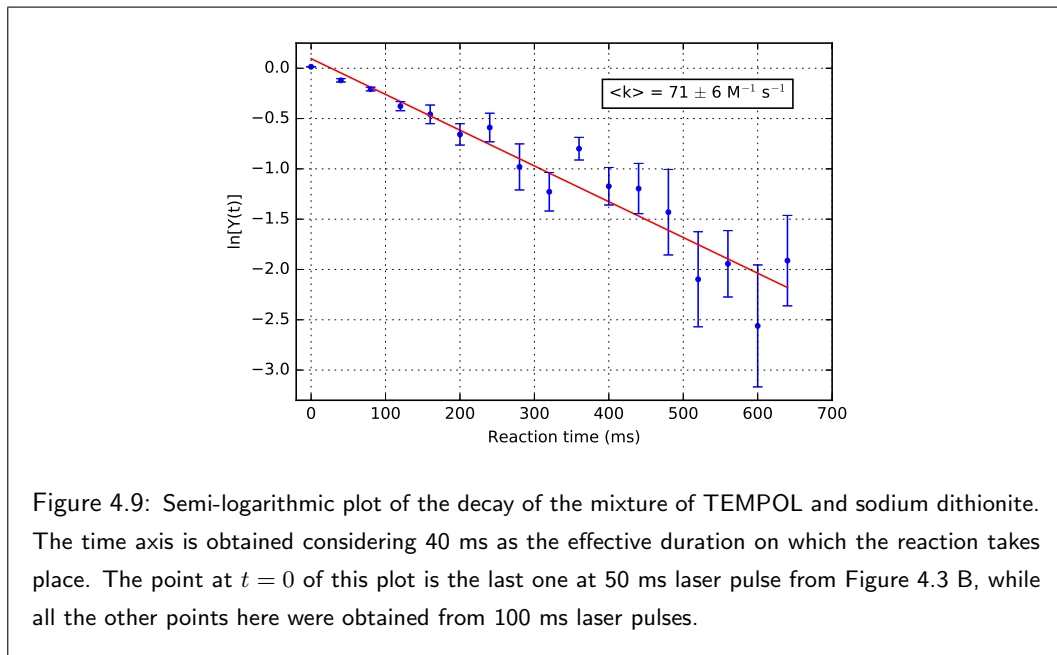


Figure 4.8: (A) Decay obtained by applying T-Cycle EPR on a mixture of TEMPOL and sodium dithionite of identical composition as for the decay of Figure 4.3. The laser pulses are applied with a duration of 5 s (or 20 s, for the last point) at a nominal power of 2.0 W, with the sample sitting at a cryostat temperature of 243 K. (B) Spectra comparison of: (a) a solution of identical composition as that of the decay (except for sodium dithionite), with the laser continuously on at 2.0 W; (b) the spectrum at 8.3 °C from the temperature calibration of Figure 4.4; (c) solution giving the decay shown in (A), before applying the laser pulses, at a cryostat temperature of 243 K; (d) the spectrum at -32.6 °C from the temperature calibration of Figure 4.4. Notice that for (A), and thus for spectra (a) and (c), the T-Cycle setup used was different with respect to the optical fiber, diode laser, and fiber connector used in this Chapter.

The temperatures responsible for the sub-second decay observed in Figure 4.3 must therefore be higher than 8 °C. Within 40 ms, the sample goes through increasing temperatures, with corresponding faster rates, all contributing to an average rate constant,  $\langle k \rangle$ , responsible for the observed decay. By taking 40 ms as the effective duration of the T-jump produced by a laser pulse of 100 ms, a new time axis is generated, with a decay up to 650 ms, as shown in Figure 4.9, where the logarithm of the  $Y(t)$  function from Figure 4.3 B is plotted versus the reaction time. Since the first five points from Figure 4.3 B correspond to laser pulses of 50 ms, while the remaining ones correspond to laser pulses of 100 ms, it is the last of the 50 ms points to be taken at  $t = 0$ . The resulting rate constant is calculated to be  $\langle k \rangle = 71 \pm 6 \text{ M}^{-1} \text{ s}^{-1}$ . Notice that varying the length of the time window by  $\pm 10\%$  leads to variations of  $\langle k \rangle$  within the calculated error of  $\pm 6 \text{ M}^{-1} \text{ s}^{-1}$ .

#### 4. EXPLORING TEMPERATURE-CYCLE EPR IN THE SUB-SECOND TIME DOMAIN



The average  $\langle k \rangle$  can be modeled as follows. Firstly, the time interval  $\Delta t = 40$  ms that the sample spends at a temperature greater than or equal to 8 °C is divided into  $n$  time elements  $\delta t$ , for whose length the sample's temperature can be considered constant. After each successive element, the decay of the 275 GHz EPR intensity of TEMPOL can be expressed as:

$$\begin{aligned}
 I_1 &= I_0 e^{-k'_1 \delta t} \\
 I_2 &= I_1 e^{-k'_2 \delta t} = I_0 e^{-(k'_1 + k'_2) \delta t} \\
 &\vdots \\
 I_n &= I_0 e^{-(k'_1 + k'_2 + \dots + k'_n) \delta t} = I_0 e^{-\frac{1}{n} \left( \sum_{i=1}^n k'_i \right) \Delta t} = I_0 e^{-\langle k' \rangle \Delta t}
 \end{aligned} \tag{4.4}$$

where  $\Delta t = n\delta t$  is the total time interval (40 ms in this case). The average apparent rate constant is thus defined as  $\langle k' \rangle = \frac{1}{n} \sum_{i=1}^n k'_i$ , from which the average rate constant is calculated through Equation 4.2 as  $\langle k \rangle = \frac{\langle k' \rangle}{[\text{S}_2\text{O}_4^{2-}]}$ .

Secondly, knowing  $k(8^\circ\text{C}) = 2 \text{ M}^{-1} \text{ s}^{-1}$ , and guessing an initial value of  $k(19^\circ\text{C})$ , it is possible to calculate  $k(T)$  at the intermediate temperatures defined by the time elements  $\delta t$ ,

assuming the  $k(T)$ 's behave according to the Arrhenius equation. By making the time step  $\delta t$  small enough so that temperature does not change during it, it is possible to calculate a set of  $k(T)$  for each guess of  $k(19^\circ\text{C})$ , by linearizing the Arrhenius equation between  $k(8^\circ\text{C})$  and  $k(19^\circ\text{C})$ . Through the linear relation between temperature and time shown in the inset of Figure 4.7, it is found that during a time interval  $\delta t = 1$  ms the temperature changes by about  $0.5^\circ\text{C}$ , which results in a negligible change in the rate constant at that  $\delta t$ , confirming that 1 ms is indeed a small enough time element. In this way, the value of  $k(19^\circ\text{C}) = 166 \pm 15 \text{ M}^{-1} \text{ s}^{-1}$ , which yields the same average rate as that of the plot of Figure 4.9 (i.e.,  $\langle k \rangle = 71 \text{ M}^{-1} \text{ s}^{-1}$ ), is found after applying the aforesaid calculations for a couple of iterations. The value of the activation energy can thus also be calculated, and is found equal to  $E_a = 280 \pm 14 \text{ kJ mol}^{-1}$ .

### 4.4 Discussion

Building on the achievements described in Chapter 3, Temperature-Cycle EPR is here taken a step further in investigating chemical kinetics on the sub-second time scales. The decay of the reduction of TEMPOL by dithionite is observed over a total laser time of 1850 ms with 275 GHz EPR, by application of laser pulses of 4.4 W nominal power and a duration of 100 ms. The decay time observed here is significantly shorter as compared to those of Chapter 3. As opposed to the experiments of Chapter 3, where the pulses applied are long enough for the sample to reach an equilibrium temperature, in the current study the pulses are much shorter, so that the system never reaches a steady state during the time the laser is on, but rather it goes through a temperature gradient during and after each laser pulse. On account of this, a quantitative analysis is performed on the temperature profile of the sample as a function of time, both during and after the application of a 100 ms long laser pulse. As a consequence, it is possible to determine a time window of about 40 ms per laser pulse within which the reaction takes place at temperatures higher than  $8^\circ\text{C}$ ; this results in a total effective laser time of 650 ms, constituting an improvement on the time resolution of the Temperature-Cycle technique of two orders of magnitude as compared to the time scales of Chapter 3. Furthermore, following such analysis it is possible to calculate the kinetic parameters of the reaction, such as the corresponding activation energy, and the rate constant as a function of temperature.

Corroboration of the analysis above comes from the comparison of the rate constant obtained here with those found in the literature for the reaction of TEMPOL and dithionite, in similar conditions as those reported here. Goldfarb *et al.* [66] reported a complete depletion of TEMPOL by dithionite to occur within 60 ms at room temperature, with a rate constant  $k(RT) = 800 \pm 100 \text{ M}^{-1} \text{ s}^{-1}$ . The most important difference between the conditions of the

present Chapter and those of [66] is the amount of glycerol in the solution, being 30% in volume there, while 50% in volume here. Further, in [66] a comparison is made with the  $k(RT) = 4000 \text{ M}^{-1} \text{ s}^{-1}$  extracted from other works for the same system [78] [79], except for the absence of glycerol in the solution. From this literature data, a 5-fold decrease of the rate constant is observed when going from 0% to 30% glycerol (i.e., from 4000 to 800  $\text{M}^{-1} \text{ s}^{-1}$ ). In the present Chapter, another 5-fold decrease is found (i.e., from 800 to 166  $\text{M}^{-1} \text{ s}^{-1}$ ), in the presence of 50% glycerol – namely, about a factor of 2 as compared to the conditions from Goldfarb *et al.*. The value of  $k(RT)$  found here is thus most reasonable as compared to the literature data, which supports the analysis performed.

It is evident from the temperature profile as a function of time following the application of a laser pulse (Figure 4.7, and also Figure 3 of Chapter 3) that the temperature decay takes a longer time than the temperature rise. This asymmetry is understandable considering that during the temperature rise, the process of laser absorption adds on the active cooling constantly acting on the sample. The sample cooling is a process determined by the thermal conductivity of the sample itself and of the medium surrounding it, namely the quartz capillary and the helium gas, which slow down the rate of the heat transfer from the sample to the environment. A limit of the T-Cycle technique in its current state is thus the heat transfer rate of the system, acting both on the heating and on the cooling of the sample following a laser pulse. Such limitation may however be lessened, as discussed below.

Improvements both on the rise and fall time of the temperature profile can be envisioned. The former can be shortened by designing a different cavity within the probe head for the 275 GHz EPR spectrometer: the current one is basically a metal cylinder featuring a grid-like bottom part that blocks a portion of the incoming beam directed onto the sample, so that only parts of the sample effectively absorb the laser. An IR-transparent dielectric cavity without such a grid-like bottom could make the laser absorption more efficient, as the whole sample would directly be irradiated by the laser beam. Also the cooling time could be reduced by acting on experimental aspects such as the sample volume and the temperature difference between the sample and the bath. By shrinking the former and/or increasing the latter, a more efficient heat transfer is to be expected, and thus a faster recovery of the temperature after the laser pulse.

### 4.4.1 Modeling of the temperature decay following a laser pulse

In order to verify the considerations mentioned above, namely whether reducing the size of the sample volume and/or increasing the  $\Delta T$  of the T-jump may accelerate the cooling process, the physical system of the present Chapter was modeled and simulated using the COMSOL

#### 4. EXPLORING TEMPERATURE-CYCLE EPR IN THE SUB-SECOND TIME DOMAIN

---

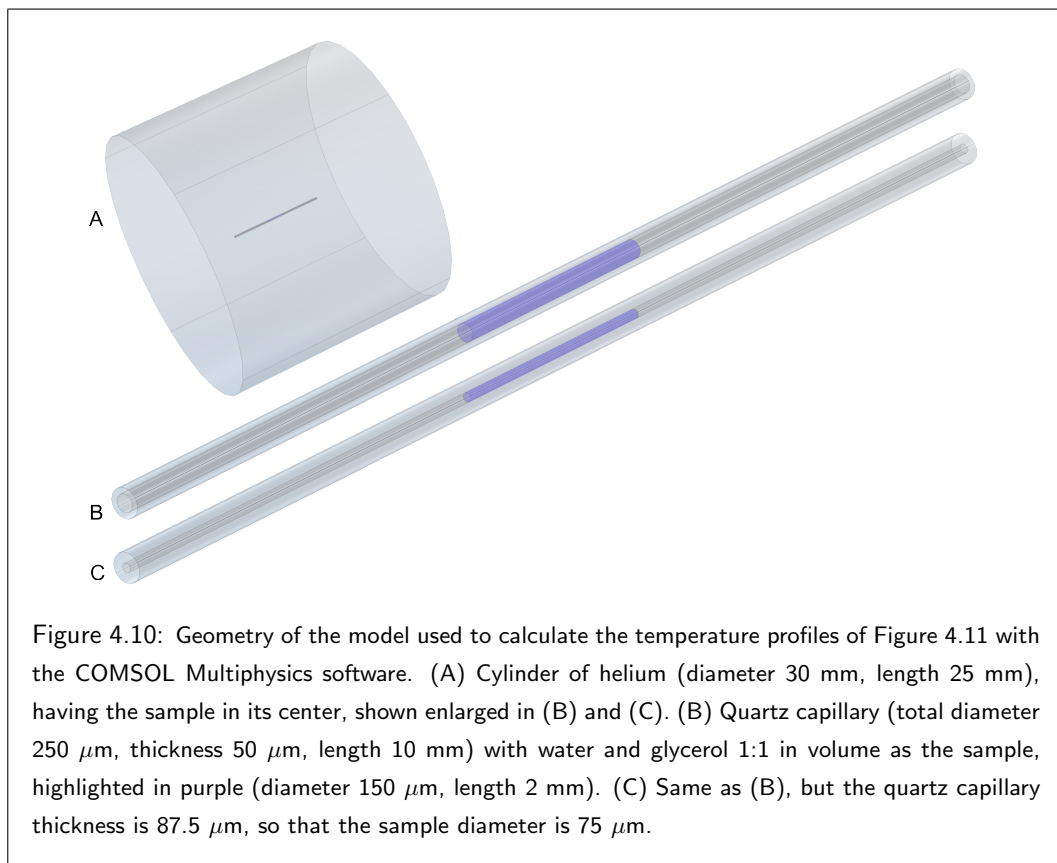
Multiphysics software (see technical details in Subsection 4.2.1). The geometry of the model was implemented with five cylinders, and is shown in Figure 4.10:

- A cylinder made of helium, much bigger than the sample size, acting as a thermal bath that simulates the cryostat;
- A much smaller cylinder made of quartz, placed in the center of the helium cylinder, representing the portion of the capillary used as a sample holder for 275 GHz experiments that is located in the spectrometer's cavity, and in the proximity thereof;
- A cylinder made of a mixture of water and glycerol 1:1 in volume, put inside the quartz cylinder, and representing the sample;
- Two cylinders made of helium, placed inside the quartz cylinder and at the two sides of the sample cylinder, used as a filling to avoid the quartz cylinder to be a solid quartz block.

The temperature at  $t = 0$  of all the cylinders was set to either 243 K or 223 K, except for the sample cylinder whose temperature was set to 303 K.

Two major simplifications were made in the model, with the purpose of simplifying the complexity of the system and saving computational time. First, no active cooling of the bath was taken into account, but rather a large volume of helium gas was created, containing the sample (of much smaller volume) at its center; refer to Figure 4.10 for the geometry used in the simulations. The volume of the helium gas used as a thermal bath ( $\sim 20$  mL), much larger than that of the sample ( $\sim 35$  nL), ensures that the temperature of the bath is maintained at 243 K (or 223 K), as the sample cools down from the initial temperature of 303 K. The second simplification regards the initial temperature of the quartz containing the sample, and the helium gas inside the quartz, on both sides of the sample: in the simulations their temperature at  $t = 0$  was set equal to that of the outer helium bath; nonetheless, more realistically a temperature gradient is present through the walls of the quartz capillary, and along the helium gas directly in contact with the sample. However physically inaccurate these two simplifications might be, in consideration of the degree of accuracy needed for the present study, they actually represent a minor deviation from the physical processes of interest here, and they allow a beneficially shorter calculation time.

Figure 4.11 shows the output of four different cases simulated with COMSOL Multiphysics, namely the sample diameter being either 150 or 75  $\mu\text{m}$  (A, C and B, D respectively), and the temperature of the bath being either 243 K or 223 K, thus the  $\Delta T$  being either 60 K or 80 K



(A, B and C, D respectively). The sample's temperature decay from the initial value of 303 K is calculated for each mesh point of the sample cylinder; since both the surface points and the inner points are evaluated, and the former are subject to a faster cooling than the latter, the result is a temperature decay represented as a band in the plots of Figure 4.11. When comparing plot A with B, and C with D, a shortening of the cooling time is observed, as a result of a four-fold decrease of the sample volume. Similarly, when comparing plot A with C, and B with D, a shortening of the cooling time is observed resulting from an increase of the  $\Delta T$  between the sample and the bath. To better illustrate these temperature decays quantitatively, Table 4.2 summarizes the average time it takes, in each case, for the sample cylinder to reach the temperature of 270 K from 303 K. The most dramatic effect can be appreciated when the sample diameter is reduced by half: for both  $\Delta T$  considered, the cooling time becomes about five times shorter. Also changing the  $\Delta T$  from 60 to 80 K reduces the cooling time significantly (of about two times), for both sample diameters considered.

#### 4. EXPLORING TEMPERATURE-CYCLE EPR IN THE SUB-SECOND TIME DOMAIN

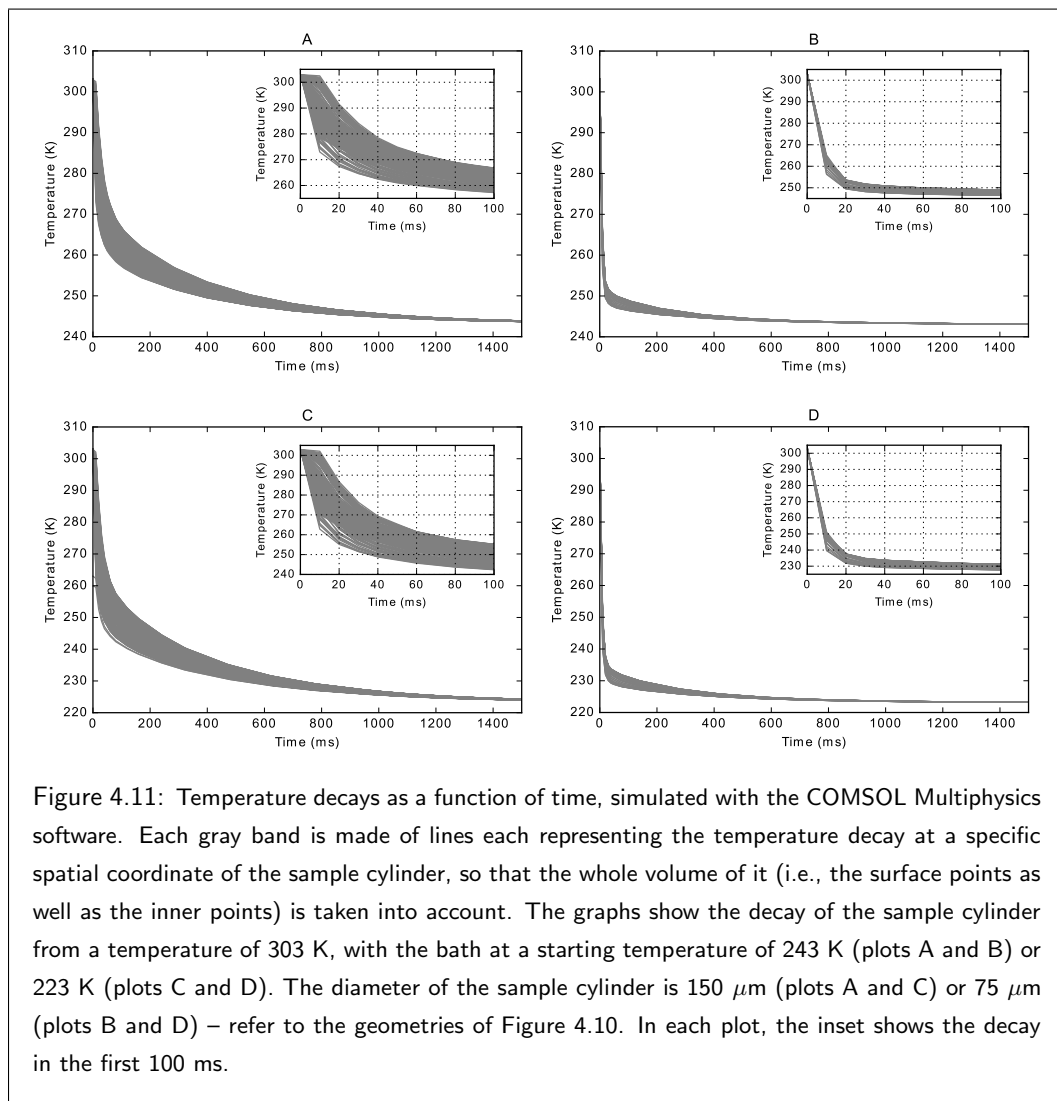


Figure 4.11: Temperature decays as a function of time, simulated with the COMSOL Multiphysics software. Each gray band is made of lines each representing the temperature decay at a specific spatial coordinate of the sample cylinder, so that the whole volume of it (i.e., the surface points as well as the inner points) is taken into account. The graphs show the decay of the sample cylinder from a temperature of 303 K, with the bath at a starting temperature of 243 K (plots A and B) or 223 K (plots C and D). The diameter of the sample cylinder is 150  $\mu\text{m}$  (plots A and C) or 75  $\mu\text{m}$  (plots B and D) – refer to the geometries of Figure 4.10. In each plot, the inset shows the decay in the first 100 ms.

From the simulations shown above it thus appears that it is possible to improve the current T-Cycle technique as far as the time for the cooling of the sample is concerned, at least by acting on two factors. One is the reduction of the sample volume, and therefore the increase of the thickness of the capillary walls; this, however, comes at the cost of a smaller signal, which might constitute a problem for low-concentrated samples. Moreover, reducing the sample diameter implies having a shorter optical path for the laser absorption, which might result in a less efficient laser-induced heating, as the sample's absorbance scales with the path length

$\Delta T$	$d = 150 \mu\text{m}$	$d = 75 \mu\text{m}$
60 K	$\langle t_A \rangle = 44 \text{ ms}$	$\langle t_B \rangle = 8 \text{ ms}$
80 K	$\langle t_C \rangle = 23 \text{ ms}$	$\langle t_D \rangle = 5 \text{ ms}$

Table 4.2: Variations of the average time ( $\langle t \rangle$ ) it takes the sample to reach the temperature of 270 K starting from 303 K, by changing two parameters in the simulations: the diameter ( $d$ ) of the sample cylinder, and the temperature difference ( $\Delta T$ ) between the sample and the bath. The subscripts A, B, C, and D refer to the plots of Figure 4.11, where the  $\langle t \rangle$ 's are taken from.

according to the Lambert-Beer law. The other factor is the increase of the  $\Delta T$  between the sample and the bath, or, in other words, the increase of the T-jump. Both factors contribute to a significant reduction of the cooling time of the sample, which thus in principle enables an even better time resolution.

## 4.5 Conclusions

In this Chapter, the reaction time scale accessible by Temperature-Cycle EPR was downsized to a few hundreds of milliseconds, rendering this technique apt for kinetic and dynamic studies of a great deal of chemical and biological processes. Starting from the time scale of minutes achieved in Chapter 3, where characteristic times of about 100 seconds were attained, a much faster decay was shown here, with a characteristic time of less than 300 milliseconds, which constitutes an improvement of two orders of magnitude. In addition to the increased time resolution of the method, the analysis of the time profiles of the sample's temperature upon application of a laser pulse leads to the determination of the reaction's kinetic parameters, namely its activation energy and the rate constant as a function of temperature. Furthermore, the feasibility of manual mixing of the reagents at temperatures well below 0 °C represents an attractive alternative to other techniques, such as Rapid Freeze-Quench or flow methods.

In its current state, Temperature-Cycle EPR offers the advantages of high-frequency EPR (such as high spectral resolution, and high sensitivity) with a time resolution already optimal for a wide range of (bio)chemical systems. Given the reaction time window of about 40 ms with which it is possible to follow a kinetic process with the present setup, a reaction with a characteristic time as short as 100 ms would be perfectly within reach. Additionally, in studies whose goal is the investigation of the evolution of paramagnetic reaction intermediates rather

#### 4. EXPLORING TEMPERATURE-CYCLE EPR IN THE SUB-SECOND TIME DOMAIN

---

than quantitative kinetics, the present setup can be employed in the time regime of tens of milliseconds.

However powerful the T-Cycle technique already is in the present, there is room to substantial improvements, particularly regarding the time resolution attainable. By acting on certain experimental parameters, such as reducing the sample volume and/or increasing the temperature difference between the sample and the cryostat, the result is a more efficient heat transfer, which is the main limitation in the cooling phase of the sample, and thus a shorter reaction time per laser pulse. Calculations performed on a model system suggest that the cooling of the sample could occur one order of magnitude faster if the sample diameter is halved as compared to the current setup, and the temperature of the cryostat is set 20 °C lower. An improved heat transfer, however, represents an obstacle to the heating of the sample, which could anyway be circumvented by devising a setup that allows a more efficient light absorption by the sample, such as a probe head with an IR-transparent dielectric cavity without a grid-like bottom that blocks part of the laser beam.

As an outlook for future developments on T-Cycle, the following considerations are advanced. With the laser-induced T-jump of  $\sim 50$  °C of the present Chapter, the temperature of  $\sim 19$  °C is reached within 100 ms. Since the increase in temperature is linear with time during a laser pulse, with a laser-induced T-jump twice as big (100 °C, shown to be possible in Chapter 3), the same temperature would be reached in as little as 50 ms, to which corresponds an even shorter reaction time per pulse. Although dealing with faster reactions might pose a challenge in terms of the manual mixing of the reagents with the method described in this Chapter, the combination of a more efficient laser absorption with a more efficient cooling of the sample can open the doors for T-Cycle EPR to kinetic investigations in time regimes of a few tens of milliseconds, if not less.



